

High-efficiency resonant amplification of weak magnetic fields for single spin magnetometry at room temperature

Luka Trifunovic¹, Fabio L. Pedrocchi^{1,2}, Silas Hoffman¹, Patrick Maletinsky¹, Amir Yacoby^{3,4} and Daniel Loss^{1*}

Magnetic resonance techniques not only provide powerful imaging tools that have revolutionized medicine, but they have a wide spectrum of applications in other fields of science such as biology, chemistry, neuroscience and physics. However, current state-of-the-art magnetometers are unable to detect a single nuclear spin unless the tip-to-sample separation is made sufficiently small. Here, we demonstrate theoretically that by placing a ferromagnetic particle between a nitrogen-vacancy magnetometer and a target spin, the magnetometer sensitivity is improved dramatically. Using materials and techniques that are already experimentally available, our proposed set-up is sensitive enough to detect a single nuclear spin within ten milliseconds of data acquisition at room temperature. The sensitivity is practically unchanged when the ferromagnet surface to the target spin separation is smaller than the ferromagnet lateral dimensions; typically about a tenth of a micrometre. This scheme further benefits when used for nitrogen-vacancy ensemble measurements, enhancing sensitivity by an additional three orders of magnitude.

In recent years, a great deal of experimental effort has been put into improving magnetic detection schemes. At present, Hall sensors and superconducting quantum interference device (SQUID) sensors are among the most sensitive of magnetic field detectors^{1,2}. A great deal of success has also been achieved with magnetic resonance force microscopy, where the force between a magnetic tip and the magnetic moment under investigation is exploited to detect single electron spins, achieving a resolution of a few cubic nanometres^{3–5}. However, the very low temperatures that are required for such schemes represent a considerable drawback to imaging systems in many biological environments.

Nitrogen vacancy (NV) centre spins are also very good candidates for magnetometry, boosting sensitivities up to a few nT Hz^{-1/2} at room temperature^{6–11} and with sub-nanometre spatial resolution, thereby permitting three-dimensional imaging of nanostructures⁷. These results are realizable due to the amazingly long coherence times of NV centres at room temperature and the ability to non-invasively engineer an NV-magnetometer very close to the magnetic sample. Although impressive, current state-of-the-art technology¹² is unable to detect a single nuclear spin unless the tip-to-sample separation is made sufficiently small¹³. Achieving such sensitivity would revolutionize magnetic imaging in chemical and biological systems by facilitating the atomic resolution of molecules.

In this Article we propose an experimental realization of NV-magnetometers that does not rely on the cubic dependence of sensitivity on the tip-to-sample separation, and is sensitive enough to detect a single nuclear spin within 10 ms of data acquisition at room temperature. This can be achieved by introducing a ferromagnetic particle between the spin that needs to be detected (hereon termed a ‘qubit’) and the NV-magnetometer. (Note that we call the target magnetic moment a ‘qubit’ solely for convenience of nomenclature—our scheme does not rely on the

quantum nature of the magnetic moment we aim to measure.) When excited on resonance by the driven qubit, the macroscopic ferromagnetic spin begins to precess, which, in turn, amplifies the magnetic field felt by the NV centre. By resonantly addressing the qubit and using a ferromagnetic resonator as a lever, our set-up, in contrast to existing schemes, is particularly advantageous because the nuclear spin need not lie within a few nanometres of the surface¹⁴, but instead can be detectable at all distances smaller than the ferromagnetic particle (FM) lateral dimensions. Furthermore, although related existing schemes rely on the quantum nature of a mediator spin¹⁵, our proposal is fully classical. With these unique features, our scheme provides chemically sensitive spin detection.

Set-up

The standard experimental set-up, yielding the most accurate NV-magnetometers (for example, ref. 7), consists of an NV centre near the target qubit and two distinct microwave sources that independently control the NV centre and qubit so that double electron–electron (electron–nuclear) resonance, DEER (DENR), can be performed. We extend this set-up by including a macrospin FM between the NV-magnetometer and the qubit we want to measure (Fig. 1). A recent experiment^{16,17} demonstrated that there is no significant quenching of the NV centre photoluminescence in the presence of the FM. On the other hand, due to the stray field of the FM, the qubit energy-splitting and therefore the frequency ω_q at which the qubit responds resonantly is strongly modified. One needs first to characterize the FM stray field in order to be able to control the qubit by, in our case, applying π -pulses. (Note that, instead of performing the qubit control resonantly, one can make use of ‘adiabatic passage’¹⁸, wherein triangular pulses are applied in lieu of square pulses. In such a set-up, knowledge of the exact value of the qubit Zeeman splitting, and therefore the FM stray

¹Department of Physics, University of Basel, Klingelbergstrasse 82, Basel CH-4056, Switzerland. ²JARA Institute for Quantum Information, RWTH Aachen University, Aachen D-52056, Germany. ³Department of Physics, Harvard University, Cambridge Massachusetts 02138, USA. ⁴Condensed Matter Chair, Department of Physics and Astronomy, University of Waterloo, Canada. *e-mail: daniel.loss@unibas.ch

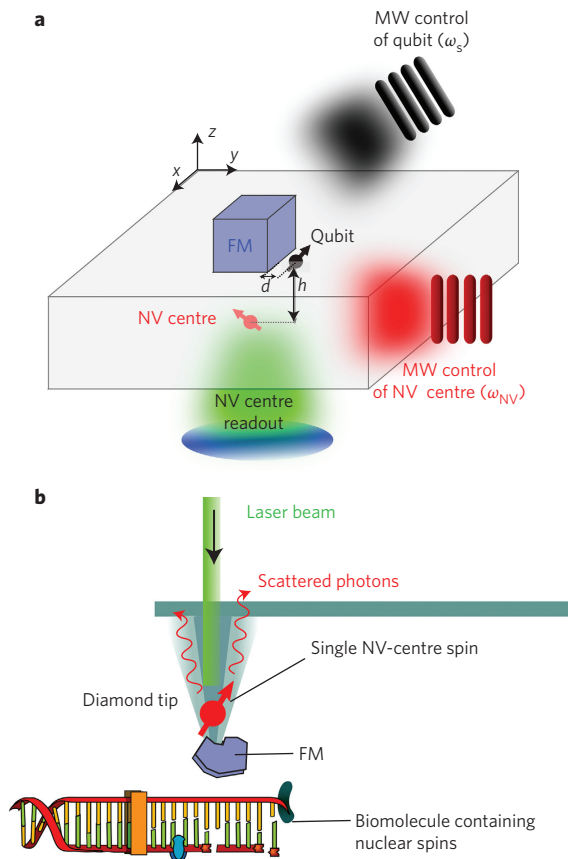


Figure 1 | Set-up. **a**, Detailed illustration of the set-up. ‘FM’ denotes the ferromagnetic particle, which is placed on top of a diamond surface containing the NV centre (red), which is used as a magnetometer. The qubit (black) to be measured lies close to the top surface of the FM. The set-up also includes separate microwave (MW) controls of the qubit (black) and NV centre (red), with resonance frequencies ω_s and ω_{NV} , respectively. The ferromagnetic resonance frequency ω_F is assumed to be different from both ω_s and ω_{NV} . The NV centre is read out optically with a green laser. **b**, A slightly modified version of the set-up with the NV centre and the FM on a tip. For simplicity the two driving fields are omitted.

field, is not needed.) Treating the ferromagnet as a single classical spin, the Hamiltonian of this system is given by^{19,20}

$$H = KV(1 - m_z^2) + M_F V b m_z - \mu_s \mathbf{n}_s(t) \cdot \mathbb{B}_F \mathbf{m} \quad (1)$$

where \mathbf{m} is the normalized magnetization of the FM, M_F is the saturation magnetization of the FM, and V is its volume. We assume uniaxial anisotropy in the FM with the anisotropy constant, $K > 0$, composed of both shape and crystalline anisotropy, with an easy axis along z . An external magnetic field b is applied along the z axis. The magnetic moment of the qubit is μ_s and $\mathbf{n}_s(t)$ is its polarization at time t . The 3×3 -matrix \mathbb{B}_F is defined as $(\mathbb{B}_F)_{ij} = \mathbf{B}_F^j(\mathbf{r}_s) \cdot \mathbf{e}_i$, where $\mathbf{B}_F^j(\mathbf{r}_s)$ is the stray field produced by the FM at the position of the qubit, \mathbf{r}_s , when the FM is polarized along the j -axis for $j = x, y$ or z . The Hamiltonian of the qubit is not explicitly written as its polarization is completely determined by the externally applied static and time-dependent microwave field and the stray field of the FM. For example, in equilibrium, the ground state of the qubit is polarized along the total static field acting on it $\mathbf{n}_s = (\mathbf{b} \pm \mathbb{B}_F^z) / |\mathbf{b} \pm \mathbb{B}_F^z|$ when $m_z = \pm 1$. Although in the following we take V small enough to approximate the FM as a monodomain, our analysis and therefore our results, are amenable to including the effects of magnetic texture.

Using two independent microwave sources we apply a train of π -pulses first to the qubit and subsequently a Carr–Purcell–Meiboom–Gill (CPMG) pulse sequence^{21,22} to the NV-centre (Fig. 2). As the qubit is pulsed it will drive the FM at the frequency of the pulse sequence π/τ , where τ is the time between the application of two subsequent π -pulses. When π/τ is close to the ferromagnetic resonance (FMR) frequency, ω_F , the response of the FM becomes large and one obtains a large amplification of the magnetic field felt by the NV centre. The pulses are applied only to the qubit until the FM reaches steady-state precession. We also allow for a possible time offset, ξ , between the pulse sequences applied to the qubit and the NV centre (Fig. 2). Here, ξ may be chosen to compensate for the phase difference between the driving of the qubit and the response of the FM, thus maximizing the sensitivity of our magnetometry scheme. Because the microwave field applied to the qubit is a sequence of π -pulses, the polarization is simply $\mathbf{n}_s(t) = \mathbf{n}_s f_\tau(t)$, where $f_\tau(t)$ may take the values ± 1 according to the pulse sequence. It is worth noting that even though we excite the FMR with the inhomogeneous dipolar field of the qubit, only the lowest Kittel mode is excited, because for a small FM higher modes are separated by an energy gap that exceeds the perturbation amplitude. The macrospin approximation used in equation (1) is therefore justified.

Proposed magnetometer sensitivity

We now consider our particular scenario in which a FM is introduced at a distance d from the qubit and h from the NV-centre (Fig. 1). In this case, both the accumulated phase and the dephasing of the NV centre are modified by the presence of the FM. Because the sensitivity of our magnetometry scheme crucially depends on the series of pulses applied to the NV centre and qubit, here we detail the pulse sequence (Fig. 2). First we apply, on the qubit only, N π -pulses separated by a time interval τ , for a total time of $t' = N\tau$. During this time the FM reaches steady-state precession. Next we initialize the NV centre in state $|0\rangle$, which takes time t_p (on the order of a few hundred nanoseconds). A $\pi/2$ pulse is then applied to the NV centre, allowing it to accumulate the phase from the FM tilt stray field. Consequently, a series of N π -pulses are applied to both the NV-centre and qubit for a total interrogation time $t_i = N\tau$. Finally, we apply to the NV centre a $\pi/2$ -pulse that is, in general, along an axis in the plane orthogonal to the NV-centre axis and different from the first $\pi/2$ -pulse by angle θ . The probability that the NV centre occupies the state $|0\rangle$ or $|1\rangle$ after the pulse sequence is now a function of the accumulated phase $\varphi_{NV}(t_i)$:

$$p(n|\varphi_{NV}(t_i)) = \frac{1}{2} \left(1 + n \cos(\varphi_{NV}(t_i) + \theta) e^{-\langle (\delta\varphi_{NV}(t_i))^2 \rangle} \right) \quad (2)$$

Here, $n = \pm 1$ are the two possible outcomes when the state of the NV centre is measured, $\langle (\delta\varphi_{NV}(t_i))^2 \rangle$ is the dephasing of the NV centre and $\langle \dots \rangle$ is the expectation value in the Gibbs state. Because the accumulated phase itself depends on the value of the qubit magnetic moment μ_s , a measurement of the NV centre is a measurement of μ_s . The variance in the measured value of the NV centre can be reduced by repeating the measurement \mathcal{N} times (Fig. 2). Because, typically, $t' \ll \mathcal{N}t_i$ and therefore $t' + \mathcal{N}t_i \approx \mathcal{N}t_i$, the total measurement time is marginally prolonged by the initial pulse sequence that initialized the tilt of the FM.

Given equation (2), one may show quite generally that the sensitivity of the NV-magnetometer is given by

$$S = \frac{1}{R\sqrt{\eta}} \min_{t_i} \left[\frac{e^{\langle (\delta\varphi_{NV}(t_i))^2 \rangle} \sqrt{t_i + t_p}}{|\partial\varphi_{NV}(t_i)/\partial\mu_s|} \right] \quad (3)$$

which defines the minimum detectable magnetic field for a given total measurement time. Here, R (the measurement contrast) is

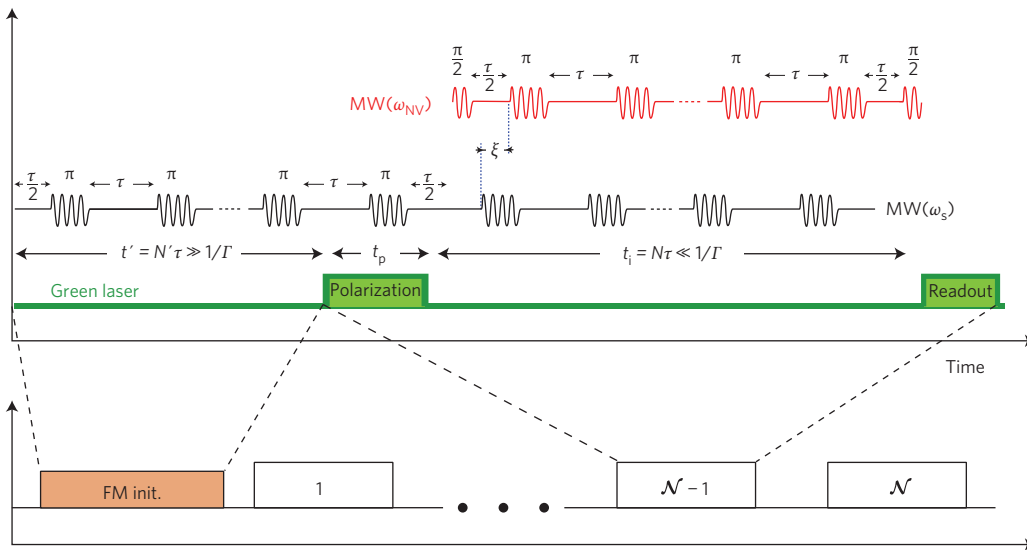


Figure 2 | The pulse sequence applied to the qubit (black) and to the NV-centre spin (red). The pulse sequence $f_{\tau}(t)$, which consists of N (N is even) π pulses, is applied to both spins, with a time offset ξ , during interrogation time $t_i = N\tau$. The measurement is repeated N times until the desired precision is achieved, as illustrated in the bottom panel. The sequence section denoted by 'FM init.' with duration $t' = N'\tau$ is the time during which the precession of the FM is being developed. We assume that the frequencies ω_s , ω_F and ω_{NV} are all sufficiently different from each other. The green laser is applied to the NV centre for initialization (polarization) and readout. The total measurement time is $t' + Nt_i \approx Nt_i$.

the relative difference in detected signal depending on spin-projection of the NV-centre spin and η is the detection efficiency which takes into account that many measurements have to be performed in order to detect a photon²³. A detailed derivation of equation (3) can be found in Supplementary Section II. The sensitivity is small (that is, 'good') when the NV-centre dephasing is small while the accumulated phase is large. When the qubit is directly coupled to the NV centre (without the FM), the dephasing time of the NV centre is given by $T_2 \approx 200 \mu\text{s}$ (refs 24,25) so that $\langle (\delta\varphi_{NV}(t_i))^2 \rangle = (t_i / T_2)^2$.

As is shown in Supplementary Section IV, given the pulse sequence described above, when $\Gamma t' \gg 1$ and $\Gamma t_i \ll 1$, where Γ is the linewidth of the ferromagnet, there is a resonant response of the FM, while the NV centre picks up non-resonant noise. As such, the ratio of the dephasing to the accumulated phase of the qubit is

minimized, thereby optimizing the sensitivity. We henceforth assume $\Gamma t' \gg 1 \gg \Gamma t_i$ in the remainder of this Article.

The accumulated phase is formally

$$\varphi_{NV}(t_i) = \gamma_{NV} \int_0^{t_i} B_{NV}(t'') f_{\tau}(t'') dt'' \quad (4)$$

where γ_{NV} is the gyromagnetic ratio of the NV. $B_{NV} \equiv |\mathbf{B}_{F,NV}^- \cdot \mathbf{n}_{NV}|$, where $\mathbf{B}_{F,NV}^{\pm} = \mathbf{B}_F^x(\mathbf{r}_{NV}) \pm i\mathbf{B}_F^y(\mathbf{r}_{NV}) [\mathbf{B}_{F,s}^{\pm} = \mathbf{B}_F^x(\mathbf{r}_s) \pm i\mathbf{B}_F^y(\mathbf{r}_s)]$, is a complex combination of the magnetic stray field for FM polarization along the x and y axes at the position of the NV centre (qubit), $\mathbf{r}_{NV}(\mathbf{r}_s)$, and \mathbf{n}_{NV} is the NV-centre polarization axis. Note that $\mathbf{B}_{F,NV}^{\pm} \cdot \mathbf{n}_{NV} (\mathbf{B}_{F,s}^{\pm} \cdot \mathbf{n}_s)$ is the FM-NV (FM-qubit) coupling constant.

Within the linear response regime and using the pulse sequence described above, and optimally choosing ξ , the expression for the phase accumulated by the NV centre when $\tau = (2k + 1)\pi/\omega_F$ (the Fourier transform of the CPMG pulse sequence has peaks at frequencies $(2k + 1)\pi/\tau$, for $k = 0, 1, \dots$, is

$$\varphi_{NV}(t_i) = \frac{4\mu_s \gamma \gamma_{NV} |\mathbf{B}_{F,s}^+ \cdot \mathbf{n}_s| |\mathbf{B}_{F,NV}^- \cdot \mathbf{n}_{NV}|}{\pi^2 (2k + 1)^2 M_F V T} t_i \quad (5)$$

where γ is the gyromagnetic ratio of the FM. k is defined such that the resonantly driven FM undergoes $2k + 1$ half-periods between consecutive π -pulses applied to the NV centre. In the optimal case we have $k = 0$, so that τ is half the period of precession of the ferromagnet. Details of the derivation of equation (5) are provided in Supplementary Section IV. It is readily observed from the above equation that $\varphi_{NV}(t_i) \sim 1/\Gamma$, which is proportional to the a.c. magnetic susceptibility of the FM on resonance, so we indeed obtain a resonant response as anticipated. Even though the phase φ_{NV} accumulated due to the FM tilt is large, the angle of the FM tilt is small ($\sim 10^{-3}$ if the qubit is a nuclear spin) because $M_F V \gg \mu_s$. We can therefore neglect the effects of the backaction of the FM tilt on the qubit, because the stray field modulation induced by the tilt is small compared with the qubit Rabi amplitude and far detuned from the qubit Larmor precession frequency (that is, $\omega_F \neq \omega_s$). Thus, the qubit is polarized along the total field $\mathbf{n}_s = (\mathbf{B}_F^+ + \mathbf{b})/|\mathbf{B}_F^+ + \mathbf{b}|$, and the scalar product $\mathbf{B}_{F,s}^+ \cdot \mathbf{n}_s$ is non-zero

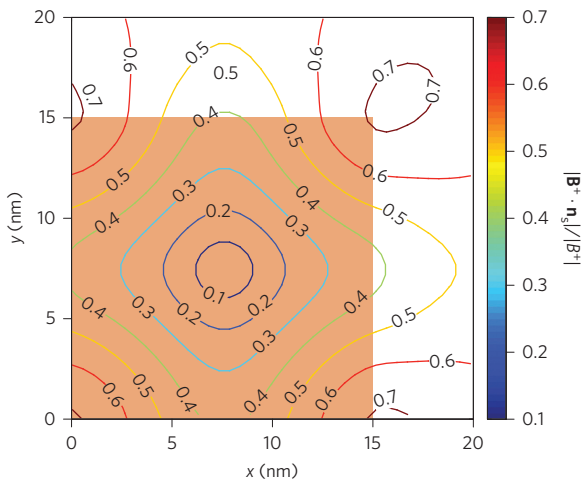


Figure 3 | Contour plot of the quantity $|\mathbf{B}^+ \cdot \mathbf{n}_s|/|\mathbf{B}^+|$ in the x - y plane 2 nm above the upper face of the cube. We assume the FM cube (orange square) has a side length of $L = 15 \text{ nm}$. The values of the stray fields are obtained from OOMMF micromagnetic simulations, taking into account the demagnetizing field.

only if the stray field of the FM tilt has a component along \mathbf{n}_s at the position of the qubit (Fig. 3). We address the optimal geometry and position of the qubit relative to the FM in the Methods ('FM geometry and demagnetizing fields').

The relevant dephasing is the maximum of the inherent dephasing of the NV centre, $(t_1/T_2)^2$ and the dephasing due to the coupling to the FM²¹

$$\beta(t_i, \tau) = \gamma_{\text{NV}}^2 \int_0^{t_i} ds S(s) \int_0^{t_i-s} dt'' f_\tau(t'') f_\tau(t'' + s) \quad (6)$$

Here, $S(s) = \langle B_{\text{NV}}(s) B_{\text{NV}}(0) \rangle$ is the autocorrelation function of the FM noise. Again, taking $\tau = (2k + 1)\pi/\omega_F$, we show in Supplementary Section IVB that

$$\beta(t_i, \tau) = \frac{4\gamma_{\text{NV}}^2 |\mathbf{B}_{\text{FNV}}^+ \cdot \mathbf{n}_{\text{NV}}|^2 k_B T}{\pi^2 (2k + 1)^2 M_F V \omega_F} t_i^2 \equiv (t_1/T_2')^2 \quad (7)$$

where T_2' is the decoherence time of the NV centre caused by the FM. Because $\beta(t_i, \tau) \sim 1/\omega_F \sim S(\omega = 0)$, the NV centre indeed accumulates non-resonant noise.

The value of the NV-centre decoherence rate when the FM volume is chosen to be as small as possible (see equation (9)) becomes $T_2'^{-1} \sim \gamma_{\text{NV}} |\mathbf{B}_{\text{FNV}}^+ \cdot \mathbf{n}_{\text{NV}}|$. Furthermore, because the optimal interrogation time is $t_1 \sim T_2'$, we obtain that for typical values of the FM stray field we are in the limit $t_1 \ll t_p$. After substituting $\langle (\delta\varphi_{\text{NV}}(t_i))^2 \rangle = \beta(t_i, \tau)$ and $\varphi_{\text{NV}}(t_i)$ from equations (5) and (7) into equation (3) and performing minimization over the interrogation time in equation (3), we find the sensitivity S_A of our magnetometry scheme

$$S_A = \frac{1}{R\sqrt{\eta}} \frac{\pi e^{\frac{1}{2}} (2k + 1) M_F V T}{\sqrt{2} \gamma |\mathbf{B}_{\text{FNV}}^+ \cdot \mathbf{n}_s|} \sqrt{\frac{\gamma k_B T t_p}{M_F V \omega_F}} \quad (8)$$

The best sensitivity is obtained when one half-period of the FM oscillation occurs over the timescale τ , that is, $k = 0$. In practice, experimental limitations, such as limitations to the qubit Rabi frequency, bound τ and therefore k from below. Thus, to achieve the resonance, one has to use $k \gg 0$ (at the expense of sensitivity) or tune the FMR frequency as described in the Methods, 'Tuning the FMR frequency'. We note that because the sensitivity in equation (8) scales as $S_A \sim \Gamma$, using low-loss FM materials like yttrium iron garnet (YIG) is crucial for achieving high sensitivities.

A few comments are in order regarding the obtained expression for the sensitivity in equation (8). First, we note that S_A is completely independent of the FM–NV coupling constant $|\mathbf{B}_{\text{FNV}}^+ \cdot \mathbf{n}_{\text{NV}}|$. This behaviour holds as long as the stray field at the position of the NV is not too weak, as otherwise a weak FM–NV coupling leads to long T_2' and we are no longer in the limit $t_1 \ll t_p$, and thus equation (8) is no longer valid. S_A therefore depends only on d and not on h (Fig. 1). Having a magnetometer with a sensitivity independent of NV positioning (note that this statement is true only in the region of space near the FM where $T_2' \ll t_p$, that is, where the FM stray field is bigger than the threshold value $B_{\text{th}} \approx 1$ G) is particularly advantageous for NV-ensemble measurements as we can use many NV centres, all with the same sensitivity (but different optimal interrogation times), and thus obtain significant improvement to the total sensitivity. Finally, S_A depends on the FM–qubit coupling constant and therefore depends on d . However, here, rather than having a sensitivity that has cubic dependence on the tip-to-sample separation, we have only a weak dependence on d because the FM stray field does not change much as long as $d \ll L \equiv V^{1/3}$ (see Methods, 'FM geometry and demagnetizing fields'). The spatial resolution of our scheme does not differ from the standard NV-magnetometry resolution⁷. In practice, the spatial resolution for detection of an isolated spin is determined

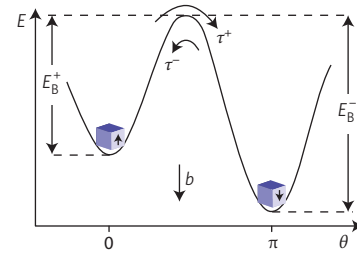


Figure 4 | The FM energy when an external field $b/b_a = 0.2$ is applied.

This describes the first two terms from the right-hand side of equation (1) of the main text, as a function of θ , where $m_z = \cos \theta$. The metastable state at $\theta = 0$ has a smaller FMR frequency compared with the case with no external field. The tunnelling time τ^+ from the metastable state has to be longer than the measurement time. We note that $E_B^+ = M_F V (b_a - b)$.

by the ratio between the magnetic field gradient and the target qubit linewidth. In the case of interacting spins there is a broadening caused by homonuclear dipolar interaction, so techniques such as magic angle spinning (MAS) should be used²⁶. As MAS is usually performed by spinning the sample in a static magnetic field, which is impractical for our scheme, one can use, instead, rotating magnetic fields²⁷ with the frequency different from ω_{NV} , ω_F and ω_s for performing MAS.

While the electron spin in a NV centre can be driven at gigahertz frequencies^{28,29}, the same driving field for a proton spin would yield a Rabi frequency in the megahertz range. Thus, the FMR frequency needs to be tuned to meet the resonance criteria. The method to achieve such a tuning is described in the Methods, 'Tuning the FMR frequency'. The idea is to use the metastable state of the FM, which has frequency that can be lowered by applying an external magnetic field (Fig. 4). For the FM to remain in the metastable state during the measurement time, the FM volume must satisfy

$$V \gtrsim \frac{\gamma k_B T}{M_F \omega_F^2} |\ln \alpha| \quad (9)$$

In the case of minimal volume, the sensitivity is given by

$$S_A = \frac{1}{R\sqrt{\eta}} \frac{\pi (2k + 1) \alpha \sqrt{e} |\ln \alpha| t_p k_B T}{\sqrt{2} |\mathbf{B}_{\text{FNV}}^+ \cdot \mathbf{n}_s|} \quad (10)$$

As noted earlier, the sensitivity of our scheme does not depend on the FM–NV coupling constant. Thus, we can take advantage of this fact to obtain an improvement to the sensitivity by a factor of $\sqrt{N_{\text{NV}}}$ when N_{NV} NV centres are used for the detection. A detailed discussion is presented in the Methods, 'NV ensemble measurements'.

Estimates

In this section we give estimates for the sensitivity S_A for two cases: with and without tuning of the FMR frequency (to the megahertz range). We also provide estimates for the case when an NV ensemble is used for the measurement. For all the estimates provided in the following we assume room temperature conditions and that the FM material is YIG, so that $\alpha \approx 10^{-5}$, $\mu_0 M_F = 0.185$ T and $K/M_F = 60$ mT (ref. 30). For simplicity, but without loss of generality, we assume that the FM has the shape of a cube for the estimates given below. For a cube and in the macrospin approximation there is no contribution from shape anisotropy.

If we tune the FMR frequency to the megahertz range, the minimum FM volume V according to equation (9) corresponds to a cube with side $L = 210$ nm. We note that because $t_1 \ll t_p \ll \tau$ (Fig. 2) one essentially performs d.c. magnetometry with the NV. Furthermore, as S_A is weakly dependent on d for $d \ll L$, we can

increase the ‘FM surface’-to-‘target spin’ separation up to values of hundreds of nanometres without decreasing the sensitivity S_A . Taking $t_p \approx 300$ ns and estimating $R\sqrt{\eta}$ from ref. 6, we obtain $S_A = 0.13 \mu_N \text{ Hz}^{-1/2}$, where μ_N is the nuclear magneton. Thus, our magnetometry scheme can detect a single nuclear spin within 10 ms of data acquisition at room temperature. For comparison, standard NV-magnetometry set-ups with state-of-the-art magnetic field sensitivity³¹, $S = 4.3 \text{ nT Hz}^{-1/2}$, need an ~ 100 times smaller tip-to-sample separation¹³ of 2.5 nm to achieve the same magnetic moment sensitivity.

For the electron spin, the minimal FM volume V according to equation (9) corresponds to a cube with side $L = 21$ nm in this case. Using the same parameters as in the previous paragraph we obtain $S_A = 0.32 \mu_N \text{ Hz}^{-1/2}$.

Typical values of the stray fields at the position of the qubit and NV centre in the limit $d, h \ll L$ for YIG are on the order of a few hundreds of gauss. The presence of a magnetic field perpendicular to the NV-centre axis can significantly limit the readout fidelity of the NV centre, and it was found that fields up to 100 G can be tolerated³². Because the sensitivity S_A does not depend on the FM–NV coupling constant, the NV should be placed in the region where the stray field $B_{F,NV}$ is less than 100 G but bigger than the threshold value B_{th} , that is, $1 \text{ G} < B_{F,NV} < 100 \text{ G}$. For $|\mathbf{B}_{F,NV}^{\pm} \cdot \mathbf{n}_{NV}| \approx 10 \text{ G}$, the decoherence time of the NV is $T_2' \approx 100$ ns (see equation (7)), which is also the value of the optimal interrogation time. Thus, because the signal amplification in our scheme far exceeds the effect of the additional decoherence it induces, even shallow NV centres^{24,25} or dense ensembles of NV centres²³ with relatively short decoherence time can be used and significantly outperform long-lived NV centres (without the FM).

Finally, we give the estimates for the case of the FMR tuned to the megahertz range and for measurements with ensembles of NV centres. As experimentally demonstrated²³, NV ensembles with a separation of ~ 10 nm between neighbouring NV centres can be achieved. Such NV ensembles have $T_2' \approx 100$ ns, but this property, as noted in the previous paragraph, does not affect the sensitivity of our scheme. We can distribute the NV centres in the volume where the stray field satisfies $B_{F,NV} > B_{th}$ and such a volume can be estimated to be a cube with side length of $1 \mu\text{m}$. Therefore, $N_{NV} \approx 10^6$, which yields an unprecedented sensitivity of $S_A = 0.13 \times 10^{-3} \mu_N \text{ Hz}^{-1/2}$.

Conclusions

We have proposed and analysed, both analytically and numerically, a modification of a standard NV-magnetometry set-up that yields a significant improvement to NV-magnetometer sensitivity. The obtained sensitivity is practically unchanged as long as the ferromagnet surface to the target spin separation is smaller than the ferromagnet lateral dimensions (typically about a tenth of a micrometre). Our scheme is based on a FM placed in close proximity to a sensing NV-centre spin. The qubit spin to be detected is then used to resonantly drive the large macrospin of the FM, giving rise to a strong, amplified stray field acting on the NV-magnetometer. Compared with existing schemes that use the quantum nature of an intermediate spin to improve sensitivity¹⁵, we stress that our scheme is fully classical and thus should be easily realizable at room temperature. All the ingredients of our scheme have already been demonstrated in separate experiments^{7,16,17,28,29,33,34}.

The magnetometric scheme including a FM, as proposed here, is a step forward to a more accurate magnetic field measurement. In particular, it enables the detection of a single nuclear spin at distances that are non-invasive to the system under study. Therefore, the proposed room-temperature magnetometry scheme opens up new venues for future analyses of previously inaccessible biological and chemical systems.

Methods

Tuning the FMR frequency. It has been demonstrated experimentally^{28,29} that the electron spin of NV centres can be coherently driven at gigahertz frequencies. For a proton spin, however, the same drive would yield Rabi oscillations in the megahertz range. Because typical FMR frequencies are in the gigahertz range, ω_F needs to be reduced in order for the proton Rabi frequency to be on resonance with the FMR frequency.

One way to decrease ω_F is to apply an external magnetic field antiparallel to \mathbf{m} (ref. 35), whereby there is a metastable state when $b < b_a$, where $b_a = K/M_F$ is the FM (crystalline and shape) anisotropy field. In Fig. 4 we plot the energy of the FM as a function of angle θ of the magnetization with respect to the easy axis, according to equation (1) of the main text. It is straightforward to show that the FMR frequency in the metastable state is $\omega_F^{\pm} = \gamma(b_a - b)$. On the other hand, the ferromagnet will relax to the thermal state on a timescale τ^+ given by the Arrhenius law $\tau^+ = \tau_0 e^{E_b/k_B T}$, where $\tau_0 \sim 1/\omega_F^{\pm}$ is the attempt time. We can ensure that the FM is initialized in the metastable state by first measuring the direction of the magnetization, applying an external magnetic field \mathbf{b} antiparallel to \mathbf{m} and checking subsequently that the FM magnetization direction is unchanged, which can be done in under 100 ps (refs 36–38).

For the ferromagnet to remain in the metastable state while the measurement is being performed, we require $\tau^+ \gg 1/\Gamma$. Indeed, the total measurement time \mathcal{T} should be larger than the FMR initialization time $t' \gg 1/\Gamma$ and smaller than the Arrhenius timescale $\tau^+ \gtrsim \mathcal{T}$ (Fig. 2). Thus, if we want to tune ω_F^{\pm} to a certain value and work at room temperature, the Arrhenius law suggests that the FM volume must satisfy

$$V \gtrsim \frac{\gamma k_B T}{M_F \omega_F^{\pm}} |\ln \alpha| \quad (11)$$

in order for the metastable state lifetime to be bigger than the measurement time. Here $\alpha = \Gamma/\omega_F^{\pm}$ is the Gilbert damping of the FM. Substituting equation (9) for the minimal volume into equation (8) of the main text we obtain

$$S_A = \frac{1}{R\sqrt{\eta}} \frac{\pi(2k+1)\alpha\sqrt{e}|\ln \alpha|t_p k_B T}{\sqrt{2}|\mathbf{B}_{F,s}^{\pm} \cdot \mathbf{n}_s|} \quad (12)$$

Compared with the sensitivity in equation (8), the above expression is independent of the FMR frequency ω_F and the FM volume V . Thus, irrespective of the choice of the frequency we work at, the same value for the sensitivity S_A is obtained. Furthermore, the only dependence on the volume is incorporated in the stray fields but, as shown in section ‘FM geometry and demagnetizing fields’, this dependence is weak in the limit $d \ll L$. The volume in equation (9) is implicitly bounded from above in order to remain in the regime where the macrospin approximation is valid.

An alternative set-up to achieve resonance between the qubit and FM is to place the NV centre and the FM on a cantilever³⁹ with resonance frequency in the gigahertz range. By driving the cantilever, we alleviate the necessity of driving the qubit at the FMR frequency as the qubit field is modulated by the oscillations of the cantilever. Because the dipolar field of the qubit decays rapidly with distance, the modulation of the qubit field achieved in this scheme is almost as big as when the qubit is driven by a microwave field (the previously described scheme for which the sensitivity estimates are given). Therefore, we conclude that the estimates for the sensitivity S_A given in section ‘Estimates’ still hold in that case.

FM geometry and demagnetizing fields. In the absence of an external magnetic field, the qubit aligns along the stray field direction of the FM, while the FM spins are aligned along the easy axis. Because $M_F V \gg \mu_s$, the FM tilt induced by the qubit is negligible. The qubit will therefore align along the direction of the stray field produced by the FM. However, for most geometries of the FM and positions of the qubit, the FM–qubit coupling constant is almost zero, that is, $|\mathbf{B}_{F,s}^{\pm} \cdot \mathbf{n}_s| \sim \mathbf{B}_{F,s}^{x,y} \cdot \mathbf{B}_{F,s}^z \approx 0$ and so the sensitivity is bad, $S_A^{-1} \approx 0$. In the following discussion, we consider our ferromagnet to be a cube of side L , but our conclusions can be straightforwardly generalized to other geometries. To gain insight into the direction and strength of the stray field, we use the well-known analogy between the stray field of a homogeneously magnetized body and an electric field produced by surface charges. Specifically, we may consider the surfaces of the cube to have charge density $\sim M_F \mathbf{m} \cdot \mathbf{s}$, where \mathbf{s} is the vector normal to the surface of the cube. Therefore, when the position of the qubit is very close to the centre of the FM surface that is perpendicular to the polarization direction (here assumed along the z axis), $\mathbf{B}_{F,s}^z$ points along the z axis. Similarly, $\mathbf{B}_{F,s}^x$ and $\mathbf{B}_{F,s}^y$ are almost aligned with the x and y axes close to the surface, respectively. Therefore, in these positions, $\mathbf{B}_{F,s}^{x,y} \cdot \mathbf{B}_{F,s}^z \sim 0$. However, this is not true near the edges of the ferromagnet. Therefore, to obtain a sensitive magnetometer, one needs (1) a ferromagnet with edges and (2) to position the qubit close to the edges. One may show analytically and numerically (Fig. 3) that $|\mathbf{B}^{\pm} \cdot \mathbf{n}_s|/|\mathbf{B}^{\pm}|$ close to the edges is about an order of magnitude bigger than close to the face centre, and that it has local maxima close to the corners of the cube.

In evaluating $\mathbf{B}_{F,s}^{x,y,z}$, we assume that the FM is homogeneously magnetized as, in the cubic geometry, one can find an analytical formula for the stray field in this case (Supplementary Section V). However, it is important to note that, due to demagnetizing fields (arising from dipole–dipole interactions in the FM), the FM

ground state is not homogeneous but rather ‘flowerlike’⁴⁰. Specifically, the canting of the spins close to the edges is more pronounced⁴¹, which modifies the FM stray field close to the edges. To account for the effects of the demagnetizing fields, we perform micromagnetic simulations in OOMMF (The code is available at <http://math.nist.gov/oommf/>). Figure 3 presents a plot of $|\mathbf{B}^+ \cdot \mathbf{n}_s|/|B^+|$ in the x - y plane 2 nm above the upper face of the cube. We find that the inclusion of demagnetizing fields changes our value of $B_{FS}^{x,y,z}$ by only $\sim 1\%$ as compared with the uniformly magnetized cube. Therefore, we expect the analytical expression for the stray field to be valid for our choice of parameters.

Because the sensitivity S_A depends on d only through the stray field at the position of the qubit, here we detail this dependence and show that the sensitivity of our magnetometry scheme is practically unchanged as d is varied. The stray field close to the cube edge (in comparison to L) is equivalent to the electric field of a set of infinite line charges. Therefore, there is a logarithmic dependence of the stray field on the distance to the edge, d , of the cube in units of L , so the sensitivity S_A is only weakly dependent on d .

NV-ensemble measurements. As noted earlier, the sensitivity of our scheme S_A does not depend on the FM–NV coupling constant. Such behaviour of the sensitivity is in stark contrast to the cubic dependence on the tip-to-sample separation of typical NV-magnetometer sensitivity. This property of S_A is very useful if we want to perform the measurements with an ensemble of NV centres, as all of them would have the same sensitivity irrespective of the actual value of the FM–NV coupling constant. Thus, we obtain an improvement of sensitivity by a factor of $\sqrt{N_{NV}}$, where N_{NV} is the number of NV centres in the ensemble. In our scheme N_{NV} is the maximum number of NV centres that we can place in the region of space around the FM where the stray field value is above the threshold B_{th} .

As the FM volume is increased, the sensitivity is decreased as $S_A \sim \sqrt{V}$ (see equation (8)). Nevertheless, in the case of an NV-ensemble measurement, increasing V leads to an increase in N_{NV} . Thus, for ensemble measurements our scheme does not lose sensitivity when the FM volume is increased, but rather the sensitivity is logarithmically improved as a result of increasing the FM–qubit coupling constant. The possibility of having a large FM without loss of sensitivity is important as it can be experimentally more feasible to work with micrometre-sized FMs.

Received 19 September 2014; accepted 13 March 2015;
published online 11 May 2015

References

- Ramsden, E. *Hall-Effect Sensors* 2nd edn (Newnes, 2006).
- Huber, M. E. *et al.* Gradiometric micro-squid susceptometer for scanning measurements of mesoscopic samples. *Rev. Sci. Instrum.* **79** (2008).
- Degen, C. L., Poggio, M., Mamin, H. J., Rettner, C. T. & Rugar, D. Nanoscale magnetic resonance imaging. *Proc. Natl Acad. Sci. USA* **106**, 1313–1317 (2009).
- Poggio, M. & Degen, C. L. Force-detected nuclear magnetic resonance: recent advances and future challenges. *Nanotechnology* **21**, 342001 (2010).
- Peddibhotla, P. *et al.* Harnessing nuclear spin polarization fluctuations in a semiconductor nanowire. *Nature Phys.* **9**, 631–635 (2013).
- Mamin, H. J. *et al.* Nanoscale nuclear magnetic resonance with a nitrogen-vacancy spin sensor. *Science* **339**, 557–560 (2013).
- Grinolds, M. S. *et al.* Subnanometre resolution in three-dimensional magnetic resonance imaging of individual dark spins. *Nature Nanotech.* **9**, 279–284 (2014).
- Staudacher, T. *et al.* Nuclear magnetic resonance spectroscopy on a (5-nanometre)³ sample volume. *Science* **339**, 561–563 (2013).
- Rondin, L. *et al.* Magnetometry with nitrogen-vacancy defects in diamond. *Rep. Prog. Phys.* **77**, 056503 (2014).
- Waldherr, G. *et al.* High-dynamic-range magnetometry with a single nuclear spin in diamond. *Nature Nanotech.* **7**, 105–108 (2012).
- Bassett, L. C. *et al.* Ultrafast optical control of orbital and spin dynamics in a solid-state defect. *Science* **345**, 1333–1337 (2014).
- Maletinsky, P. *et al.* A robust scanning diamond sensor for nanoscale imaging with single nitrogen-vacancy centres. *Nature Nanotech.* **7**, 320–324 (2012).
- Sushkov, A. O. *et al.* Magnetic resonance detection of individual proton spins using quantum reporters. *Phys. Rev. Lett.* **113**, 197601 (2014).
- Loretz, M., Pezzagna, S., Meijer, J. & Degen, C. L. Nanoscale nuclear magnetic resonance with a 1.9-nm-deep nitrogen-vacancy sensor. *Appl. Phys. Lett.* **104** (2014).
- Schaffry, M., Gauger, E. M., Morton, J. J. L. & Benjamin, S. C. Proposed spin amplification for magnetic sensors employing crystal defects. *Phys. Rev. Lett.* **107**, 207210 (2011).
- van der Sar, T., Casola, F., Walsworth, R. & Yacoby, A. Nanometre-scale probing of spin waves using single electron spins. Preprint at <http://arXiv.org/abs/1410.6423> (2014).
- Wolfe, C. S. *et al.* Off-resonant manipulation of spins in diamond via precessing magnetization of a proximal ferromagnet. *Phys. Rev. B* **89**, 180406 (2014).
- Fuchs, G. D., Burkard, G., Klimov, P. V. & Awschalom, D. D. A quantum memory intrinsic to single nitrogen-vacancy centres in diamond. *Nature Phys.* **7**, 789–793 (2011).
- Stoner, E. C. & Wohlfarth, E. P. A mechanism of magnetic hysteresis in heterogeneous alloys. *Phil. Trans. R. Soc. Lond. A* **240**, 599–642 (1948).
- Trifunovic, L., Pedrocchi, F. L. & Loss, D. Long-distance entanglement of spin qubits via ferromagnet. *Phys. Rev. X* **3**, 041023 (2013).
- Cywiński, A., Lutchyn, R. M., Nave, C. P. & Das Sarma, S. How to enhance dephasing time in superconducting qubits. *Phys. Rev. B* **77**, 174509 (2008).
- De Lange, G., Wang, Z. H., Rista, D., Dobrovitski, V. V. & Hanson, R. Universal dynamical decoupling of a single solid-state spin from a spin bath. *Science* **330**, 60–63 (2010).
- Acosta, V. M. *et al.* Diamonds with a high density of nitrogen-vacancy centers for magnetometry applications. *Phys. Rev. B* **80**, 115202 (2009).
- Ohno, K. *et al.* Engineering shallow spins in diamond with nitrogen delta-doping. *Appl. Phys. Lett.* **101**, 082413 (2012).
- Myers, B. A. *et al.* Probing surface noise with depth-calibrated spins in diamond. *Phys. Rev. Lett.* **113**, 027602 (2014).
- Puentes, G., Waldherr, G., Neumann, P., Balasubramanian, G. & Wrachtrup, J. Efficient route to high-bandwidth nanoscale magnetometry using single spins in diamond. *Sci. Rep.* **4**, 4677 (2014).
- London, P., Balasubramanian, P., Naydenov, B., McGuinness, L. P. & Jelezko, F. Strong driving of a single spin using arbitrarily polarized fields. *Phys. Rev. A* **90**, 012302 (2014).
- Fuchs, G. D., Dobrovitski, V. V., Toyli, D. M., Heremans, F. J. & Awschalom, D. D. Gigahertz dynamics of a strongly driven single quantum spin. *Science* **326**, 1520–1522 (2009).
- Yoneda, J. *et al.* Fast electrical control of single electron spins in quantum dots with vanishing influence from nuclear spins. *Phys. Rev. Lett.* **113**, 267601 (2014).
- Schryer, N. L. & Walker, L. R. The motion of 180 domain walls in uniform dc magnetic fields. *J. Appl. Phys.* **45**, 5406 (1974).
- Balasubramanian, G. *et al.* Ultralong spin coherence time in isotopically engineered diamond. *Nature Mater.* **8**, 383–387 (2009).
- Tetienne, J.-P. *et al.* Magnetic-field-dependent photodynamics of single NV defects in diamond: an application to qualitative all-optical magnetic imaging. *New J. Phys.* **14**, 103033 (2012).
- Schäfer-Nolte, E. *et al.* Tracking temperature dependent relaxation times of individual ferritin nanomagnets with a wide-band quantum spectrometer. Preprint at <http://arXiv.org/abs/1406.0362> (2014).
- Schäfer-Nolte, E. *et al.* Tracking temperature-dependent relaxation times of ferritin nanomagnets with a wideband quantum spectrometer. *Phys. Rev. Lett.* **113**, 217204 (2014).
- Smith, D. O. Static and dynamic behavior of thin permalloy films. *J. Appl. Phys.* **29**, 264–273 (1958).
- Lotze, J., Huebl, H., Gross, R. & Goennenwein, S. T. B. Spin Hall magnetoimpedance. *Phys. Rev. B* **90**, 174419 (2014).
- Julliere, M. Tunneling between ferromagnetic films. *Phys. Lett. A* **54**, 225–226 (1975).
- Lee, K.-J., Deac, A., Redon, O., Nozieres, J.-P. & Dieny, B. Excitations of incoherent spin-waves due to spin-transfer torque. *Nature Mater.* **3**, 877–881 (2004).
- Teissier, J., Barfuss, A., Appel, P., Neu, E. & Maletinsky, P. Strain coupling of a nitrogen-vacancy center spin to a diamond mechanical oscillator. *Phys. Rev. Lett.* **113**, 020503 (2014).
- Aharoni, A. *Introduction to the Theory of Ferromagnetism* 2nd edn (Oxford Univ. Press, 2001).
- Samofalov, V. N., Belozorov, D. P. & Ravlik, A. G. Strong stray fields in systems of giant magnetic anisotropy magnets. *Physics-Uspekhi* **56**, 269 (2013).

Acknowledgements

The authors thank H. Fanghor for sharing his expertise about micromagnetic simulations. This work was supported by the Swiss National Science Foundation, the National Centre of Competence in Research, Quantum Science and Technology, Diamond Devices Enabled Metrology and Sensing, Intelligence Advanced Research Projects Activity, the Defense Advanced Research Projects Agency, Quantum-Assisted Sensing and Readout programmes and the Multidisciplinary University Research Initiative, Qubit Enabled Imaging, Sensing, and Metrology. F.L.P. acknowledges support from the Alexander von Humboldt Foundation.

Author contributions

L.T. and F.P. performed the calculations and numerical simulations. L.T. and D.L. were responsible for the project planning. All the authors contributed to the discussions and writing. D.L. initiated and supervised the work.

Additional information

Supplementary information is available in the [online version](#) of the paper. Reprints and permissions information is available online at www.nature.com/reprints. Correspondence and requests for materials should be addressed to D.L.

Competing financial interests

The authors declare no competing financial interests.